Springer

Journal of Mechanical Science and Technology 23 (2009) 1261~1269

Journal of Mechanical Science and Technology

www.springerlink.com/content/1738-494x
DOI 10.1007/s12206-008-1220-0

Role of extruded texture on fatigue crack growth in a high strength aluminum alloy thick-walled cylinder †

M. A. Malik, I. Salam*, W. Muhammad and N. Ejaz

Department of Mechanical Engineering, College of Electrical and Mechanical Engineering, National University of Sciences & Technology, Peshawar Road, Rawalpindi – 46000, Pakistan

(Manuscript Received February 1, 2008; Revised June 18, 2008; Accepted December 24, 2008)

Abstract

In present study, as a basic step for modeling the fatigue behavior of an extruded Al alloy cylinder, the fatigue crack growth data of the alloy was collected in two orientations. Microstructural analysis revealed that the material had re-crystallized grains and clusters of constituent particles aligned in the direction of extrusion. Fatigue life of the samples revealed a shorter fatigue life representing a higher fatigue crack growth rate in transverse direction. The Paris constants C and m were found to be 4 x 10^{-11} and 3.4 for the transverse orientation. The same constants were found to be 2 x 10^{-10} and 2.6 for the longitudinal direction. Post fracture analysis revealed that the topographical appearance of the fractured surfaces in two orientations was different. The mechanism of crack growth was the formation of striations. The present study revealed that the texture of the constituent particles created during extrusion process has a pronounced effect on the crack growth rate in two orientations.

Keywords: Aluminum alloy; Fatigue crack growth; Paris constants; Post-fracture analysis

1. Introduction

Mechanical failure of structures and components is a serious concern in all types of industries. Almost 50-90% of all mechanical failures are due to fatigue. The fatigue failure process uses the discontinuities in the test material which act as weak links. These discontinuities normally act as the nucleation sites for crack origins. To develop a material-based and reliable life prediction methodology, there is a need to demonstrate direct link between microstructural features and fatigue performance [1].

The anisotropy in the material produces the microstructural variations in different orientations of the material. If the actual SN data are available, microstructural effects are inherently accounted for and therefore do not have to be accounted for again. Anisotropy caused by cold working gives increased SN fatigue resistance when loaded in the direction of the working than when loaded in the transverse direction. This is due to the elongated grain structure in the direction of the original cold working.

In general, the fatigue process is characterized by three distinct regions [2]. Region II normally known as the Paris region shows essentially a linear relationship between log da/dN and log ΔK. This region has received the greatest attention as it is in this region the Paris crack growth law can be applied, viz:

$$da/dN = C\Delta K^m$$

Here m is the slope of the line obtained from the above equation and C is coefficient found by extending the straight line to ΔK=1 MPa√m. Both C and m are experimentally obtained constants. The second stage prevails for an appreciable time until finally the material fails.

For a given material and environment, the fatigue

† This paper was recommended for publication in revised form by Associate Editor Chongdu Cho

*Corresponding author. Tel.: +92 51 9278046, Fax.: +92 51 9278048
E-mail address: iftikhar.salam@gmail.com

crack growth behavior is essentially the same for different specimens or components because the stress intensity factor range (ΔK) is the principal controlling factor in fatigue crack growth [3]. Thus the fatigue crack growth rate (da/dN) versus ΔK data obtained on simple specimen configurations, under constant amplitude conditions, can be used for engineering design. Knowing the stress intensity factor expression, K, for a given component and loading conditions, the fatigue crack growth life of the component can be assessed by integrating the sigmoidal curve between the limits of initial crack size and final crack size.

Aluminum alloys are of vital importance for many structural applications in automotive, aircraft and nuclear industries [4, 5]. The principal design features of these alloy systems are their high strength with low density along with high corrosion resistance. The 6000 series aluminum alloys are frequently used due to relatively high strength, good corrosion resistance and high toughness in addition to their good formability and weldability [6, 7].

Aluminum alloys generally contain constituent particles. These constituent particles are formed during the cooling process when some of the alloying elements solidify more rapidly than the aluminum [8]. These particles are inherent in the material. Investigations of the nucleation and the crack growth process in aluminum alloys have been extensively done [9-20] and the constituent particles are found to play an important role in the fatigue of aluminum alloys.

Many researchers have made experimental observations of the types of features that nucleate fatigue cracks in aluminum alloys. Generally, it was observed that the cracks were formed at debonded or broken constituent particle clusters or at particles that cracked when the material was rolled. Suresh et al. [21] have highlighted the influence of the grain structure and slip characteristics in aluminum alloys. They pointed out that microstructural effects have a strong influence on fatigue crack growth rates near threshold. Fonte et al. [11] have studied the effect of microstructure and environment on fatigue crack growth resistance of aluminum alloys and concluded that these significantly affect the process of fatigue crack growth.

In a study on aluminum alloy 2024-T3, Ali Merati [1] concluded that although constituent particles were the main fracture origins for unclad specimens, there were no clear relations between fatigue life and the fatigue subset discontinuity (particle) size, i.e. a larger discontinuity did not result in a shorter fatigue life. He also pointed out that there are factors such as grain size and orientation that could play crucial roles while determining the fatigue life. Minimizing discontinuities including the constituent particles in the aluminum alloys is a key to good fatigue resistance. In a study on an aluminum alloy AA 2026 extrusion bars, it was observed that reducing the density of constituent particles improved the fatigue resistance of the alloy [22].

The objective of the research work is to carry out theoretical and experimental investigations of an extruded aluminum alloy thick-walled cylinder under fatigue loadings. In the work presented in this study, as a basic step to achieve the objective, the fatigue crack growth data of a high strength Al-Mg-Si alloy AA 6061-T6 was collected using middle tension M(T) specimens. Samples from an extruded thick-walled cylinder were prepared in two orientations; CR (transverse) and LR (longitudinal) and tested under constant amplitude loads according to the standard ASTM E 647. The loading conditions on CR and LR samples represent the hoop and axial stress on the cylinder, respectively. Prior to fatigue testing, the microstructural analysis was conducted with the help of optical and scanning electron microscopes and the mechanical properties were determined. After the fatigue tests, the topographical features of the fractured surfaces were examined using scanning electron microscope (SEM).

2. Material and experimental procedure

2.1 Material characterization

The component under investigation was extruded thick-walled cylinder of aluminum alloy. The material of the cylinder was characterized before fatigue testing. This includes the chemistry, microstructural evaluation and the mechanical properties in monotonic tensile loading. The tests were conducted in two orientations; longitudinal (along the extrusion direction) and transverse (perpendicular to the extrusion direction).

2.1.1 Chemical composition

The chemical composition of the extruded material is given in Table 1. The material confirms the specifications of aluminum alloy AA 6061. The major constituents of the alloy are Al, Mg and Si.

Table 1. Nominal composition of the extruded material.

Element	Wt. %
Mg	0.94
Si	0.64
Fe	0.20
Cu	0.19
Cr	0.10
Mn	0.06
Al	Bal.

2.1.2 Mechanical properties

The material was in T6 heat treatment condition. Prior to fatigue testing, tensile tests were conducted according to ASTM B557M standard and the tensile properties of the material were determined.

2.1.3 Microstructural analysis

Metallographic sections were prepared using standard procedures and optical and scanning electron microscopes were used to examine the microstructural features of the alloy. Samples were studied in polished as well as etched conditions, in two orientations. Etching was done in 3% HF solution to reveal the grain size and their orientation. Energy Dispersive X-ray (EDX) analysis of the constituent particles was conducted in SEM.

2.2 Fatigue crack growth testing

2.2.1 Sample preparation

Fatigue crack growth tests were performed on middle tension M(T) specimens. Samples were cut from the extruded cylinder and machined to final dimensions according to the standard ASTM E 647 [23]. Samples were prepared in two orientations; CR and LR. These orientations refers to the standard ASTM E 399 which provides the crack plane orientation code for bar and hollow cylinder. The notch direction in the two sets of samples was such that the crack propagation in both the cases was along the radial direction of the cylinder. The samples CR and LR under loading conditions represent the hoop and axial stress on the cylinder. The samples were subjected to mechanical grinding and subsequently fine polishing with 1 μm alumina powder to minimize the surface roughness effects. Due to the limitation of wall thickness, the sample in CR direction was a bit smaller than the sample in LR direction. However, the dimensions of both the samples were within the range as given in the standard ASTM E 647. The dimensions of the CR sample are given in Fig. 1. The same for the LR sample were 2.5 mm thickness and 20 mm width.

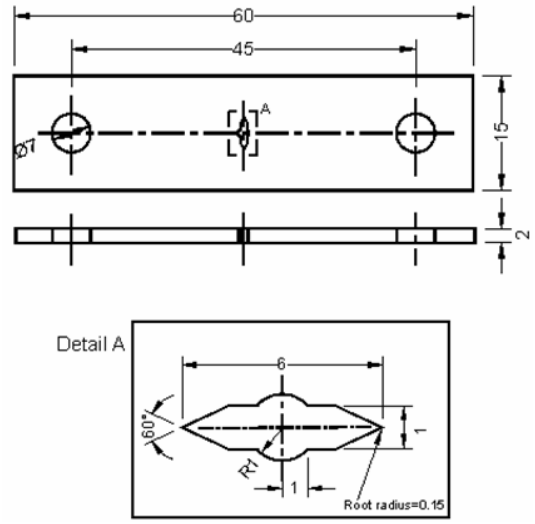

Fig. 1. Dimensional details of the M(T) sample - CR direction (dimensions in mm).

2.2.2 Test parameters

The fatigue crack growth experiments were performed on a servo-hydraulic testing machine in accordance with the standard ASTM E 647 [23]. The tests were conducted in tension-tension mode under constant amplitude loading with R ratio 0.1. A sinusoidal waveform was applied at a loading frequency of 10 Hz. The tests were conducted at maximum stress levels representing 10 to 40% of the yield strength of the material. A total of 12 samples for each CR and LR orientations were tested. A pre-crack length of 1 mm was maintained as per requirement of the standard. The data from the start of the pre-crack to 1 mm and up to the failure was recorded. Crack length was measured with the help of traveling microscope at a magnification of 100 X. The resolution of the measuring system was 0.01 mm. The tests were interrupted for short times to measure the crack length. During testing, the number of cycles and crack extension data were recorded until failure. The number of cycles to failure was taken as the fatigue life of the samples. Testing was conducted in air at 20°C and approximately 50% relative humidity.

2.3 Fractography

All the failed specimens were inspected using a stereo microscope. After the inspection the fractured surfaces of the specimens were cut using a cutting tool, reducing the height of the samples, cleaned in acetone and examined in SEM. The topographical features were studied to understand the interaction of fatigue crack with the constituent particles and the grain structure. The images of the important features of the fracture surfaces were recorded. Inspection was conducted with the electron beam in alignment with the applied axial force.

3. Results and discussion

3.1 Microstructural analysis

Fig. 2 shows the SEM micrograph of the etched sample in longitudinal direction. The constituent particles are visible preferably along the grain boundaries and aligned along the extrusion direction. Examination of these particles at high magnification revealed that clusters of particles were present at these locations. It seems that these particles were formed during solidification and fractured in fragments and aligned along the axis of the cylinder during extrusion. EDX analysis showed that the alloy frequently contained the particles rich in Al, Fe, Si, Cr and Mn. However, particles rich in Al, Mg and Si were also present in the alloy. The area fraction of the particles in two orientations is given in Table 2.

Fig. 3 shows the microstructure of the alloy in longitudinal and transverse directions. These micrographs represent the plane in which crack propagation had taken place during fatigue testing. The etched microstructure revealed that it consists of recrystallized grain structure. It seems that the grains elongated along the extrusion direction during extrusion process. These elongated grains recrystallized during the heat treatment after extrusion. The grain size of the alloy in longitudinal and transverse directions is given in the Table 2. The results show that the recrystallized grains are almost equiaxed.

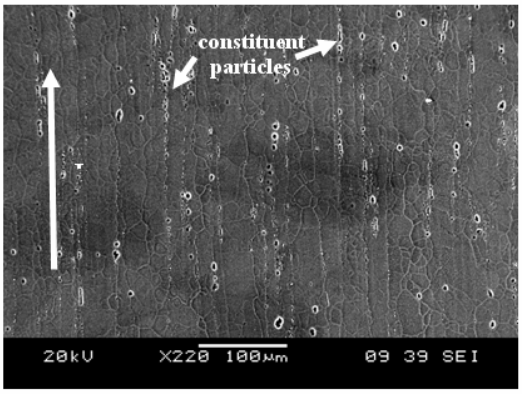

Fig. 2. SEM micrograph of the alloy showing the constituent particlesin longitudinal direction.

3.2 Mechanical properties

The mechanical properties of the extruded alloy in two orientations determined at a strain rate of 3 x 10^{-5} /s are given in Table 3. The analysis of the results presented in Table 3 shows that the yield strength and ultimate tensile strength of the material in the two orientations were not different. However, the difference in the deformation behavior was significant.

Table 2. Quantitative microstructural analysis.

Microstructural feature	Orientation	
	Longitudinal	Transverse
Grain size, µm	13 ± 5	15 ± 4
Particles area fraction, %	6.5 ± 1.0	5.1 ± 1.2

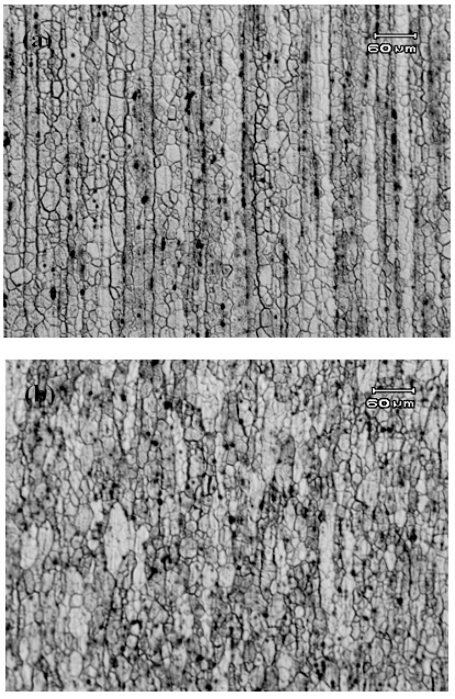

Fig. 3. Optical micrographs revealing the microstructure of the alloy in a) longitudinal and b) transverse directions.

Table 3. Nominal mechanical properties of extruded alloy.

Properties	Orientation	
	Longitudinal	Transverse
0.2% Yield strength, MPa	324	322
Ultimate tensile strength, MPa	354	353
Elongation, %	16	9
Reduction of area, %	50	24
Elastic modulus, GPa	71	71
Hardness, HV	115	115

These properties indicate that the recrystallized grain structure has eliminated the effect of texture on the yield and tensile strengths of the material. However, the texture produced by the clusters of the constituent particles was not eliminated by subsequent heat treatment processes and that reduced the elongation and reduction of area in the transverse direction.

3.3 Fatigue test results

3.3.1 Fatigue life of the samples

Tables 4a and 4b provide the results of the stress range (ΔS) and the number of cycles to failure (N_f) for the samples tested in CR and LR orientations, respectively. The scatter in the results is also given in the table and it should be noted that the difference in the fatigue life in two orientations is beyond the limit of the scatter at any stress level. It's worth mentioning here that although the sample size in the two orientations was a bit different, however the loading conditions during testing were ensured to be the same for both the orientations. As already mentioned that for a given material and environment, the fatigue crack growth behavior is essentially the same for different specimens because the stress intensity factor range is the principal controlling factor in fatigue crack growth [3]. Thus the da/dN versus ΔK data obtained from the samples, under constant amplitude conditions, can be compared and used for engineering design.

Table 5 shows the comparison of the data for two orientations. A statistical regression analysis of the experimental data was conducted using the Microsoft Excel software which provides the different regression types. The plots of the SN data were obtained and the trendlines added to the curves. These trendlines are used to graphically display the trends in data

Table 4. (a) SN data for CR orientation.

Sample #	ΔS (MPa)	N_fCR (cycles)	Average N_fCR (cycles)	% scatter*
1.	129	4037	3505	21
2.		2973		
3.	112	5078	5054	1
4.		5029		
5.	97	8376	8305	1
6.		8233		
7.	82	12195	13988	18
8.		15780		
9.	63	28653	29343	3
10.		30032		
11.	47	99521	-	-
12.	31	480179	-	-

*Standard deviation / Average N_f x 100

Table 4. (b) SN data for LR orientation.

Sample #	ΔS (MPa)	N_fLR (cycles)	Average N_fLR (cycles)	% scatter
1.	129	8264	7667	11
2.		7070		
3.	112	9986	9635	5
4.		9283		
5.	97	15507	14036	15
6.		12565		
7.	82	26550	23865	16
8.		21179		
9.	63	63672	64609	2
10.		65546		
11.	47	264476	-	-
12.	31	600000 +	-	-

+ run out

Table 5. Comparison of the SN data for two orientations.

#	ΔS (MPa)	Number of cycles to failure, N_f			
		N_fCR	N_fLR	N_fLR - N_fCR	% increase
1.	129	3505	7667	4162	119
2.	112	5054	9635	4581	91
3.	97	8305	14036	5731	69
4.	82	13988	23865	9877	71
5.	63	29343	64609	35266	120
6.	47	99521	264476	164955	166
7.	31	480179	600000 +	119821 +	-

and depends on the type of the data used. When the data is fitted to a trendline, Excel automatically calculates its R-squared value. R-squared (R^2) value is an indicator from 0 to 1 that reveals how closely the estimated values for the trendline correspond to the actual data. A trendline is most reliable when its R^2 value is at or near 1. This value is also known as the coefficient of determination.

The analysis of the data presented in Table 5 shows that the data is best fitted with the power law relationship and provides coefficient of determination, R^2 equal to 0.9899 and 0.9857 for CR and LR orientations, respectively. The data shows that in both the orientations, fatigue lifetime increases as the stress amplitude decreases. Table 5 clearly revealed a shorter fatigue life of the samples prepared in CR orientation. The percent increase in the number of cycles to failure in LR orientation at any stress level is also shown in the table. The difference between the two orientations is more evident at lower stress levels, a possible explanation of which is the texture of the constituent particles. Clusters of aligned particles in CR orientation were present in the direction perpendicular to the loading axis and more favorably oriented for crack initiation and growth. The shorter fatigue life is of serious concern because in this orientation the hoop stress in the cylinder has about twice the value of the axial stress [24].

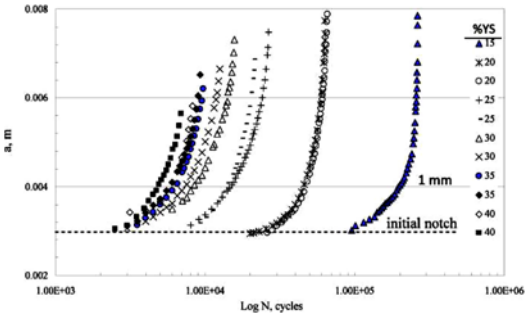

Fig. 4. Plot of the crack length versus the number of cycles for CR orientation.

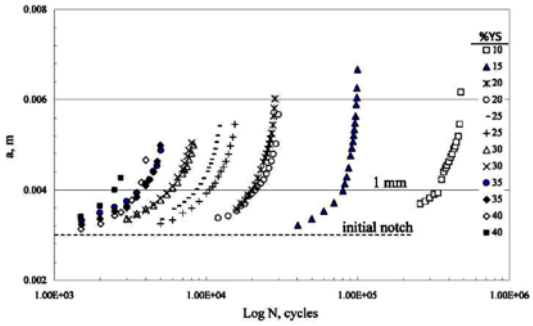

Fig. 5. Plot of the crack length versus the number of cycles for LR orientation.

3.3.2 Crack extension

Plots in Figs. 4 and 5 show the crack length versus the number of cycles for CR and LR orientations, respectively.

The legends indicate the maximum stress level in percent of yield strength of the material. The data covers the complete range from start of the crack at the notch up to the specimen failure. A pre-crack length of 1 mm is marked on the graph. Above pre-cracking line the curve becomes linear representing a smooth increase of crack length with the increase in number of cycles. Effect of the stress level on the onset of crack from the notch and the crack extension up to failure is clear from the plots. Both the number of cycles to start the crack from the notch and the maximum value of the crack length up to failure increase with the decrease in the stress level. Comparing the two graphs in Figs. 4 and 5, it is evident that in CR orientation, at the same stress level, the crack started earlier and the maximum value of the crack length is smaller.

3.3.3 Fatigue crack growth curve

The variations of fatigue crack growth rates with the ΔK are shown in Fig. 6 for the CR and in Fig. 7 for the LR samples. These figures show the data obtained from all the samples tested at different stress levels. The plots on log-log scale indicate typical sigmoidal shape. The experimental values of the Paris constants were obtained from these plots and the results are given in Table 6.

Although the tensile strength of the material in two orientations was nearly the same, the fatigue crack growth rate in the CR orientation was higher as compared to LR, which can be attributed to the presence of favorably oriented clusters of constituent particles.

It should be noted that within same material the crack growth rates in two different orientations is markedly different and should be considered to get the optimized results. Thus the present study concludes that the pattern of distribution of the constituent particles created during extrusion process has a pronounced effect on the crack growth rate.

Table 6. Paris constants obtained from the experimental data.

Alloy	Form	Orientation	C (m/cycle)	m
AA 6061-T6	Extrusion	CR	4×10^{-11}	3.4
		LR	2×10^{-10}	2.6

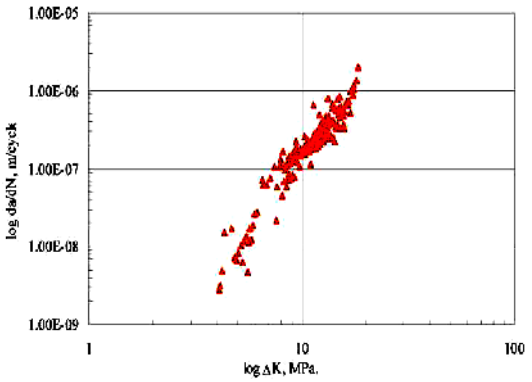

Fig. 6. Fatigue crack growth rate curve for CR orientation.

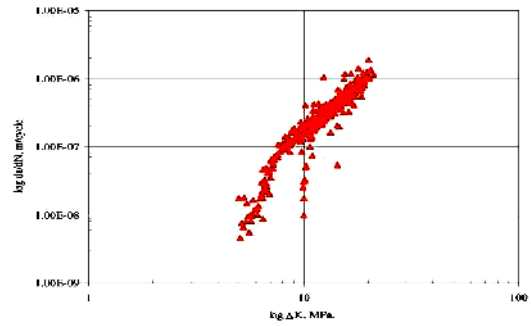

Fig. 7. Fatigue crack growth rate curve for LR orientation.

3.4 Post-fracture analysis

Post fracture analysis in SEM revealed that the fracture appearance changed with the sample orientation and resembles the respective microstructural features of the alloy. Fig. 8 shows the SEM micrographs of the samples tested at ΔS equals 63 MPa for the two orientations at intermediate ΔK. The corresponding numbers of cycles to failure for these samples were 28653 and 63672, respectively. The SEM images of the two fractured surfaces show a faceted fracture. The crack propagated along the crystallographic planes. At higher magnifications striations were found on the entire fatigue fracture surface. Their spacing varied from near threshold to the stage III crack growth region. This indicates that the general mechanism of crack growth was the formation of

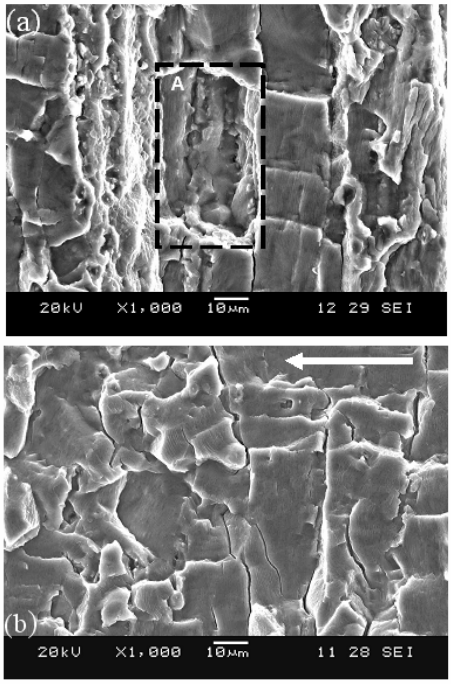

Fig. 8. SEM micrographs of fatigue fractured surfaces of a) CR and b) LR orientation at intermediate ΔK (arrow indicates crack growth direction).

striations. However, clusters of constituent particles, as were observed during microstructural analysis were found on the fracture surfaces of the CR orientation; region A in Fig. 8(a). It can be seen that the mechanism of crack growth locally changed in the regions containing high density of these particles. The higher crack growth rate found in the CR direction can be attributed to this phenomenon.

4. Summary and conclusions

In present study, the fatigue crack growth data of a high strength Al-Mg-Si alloy AA 6061-T6 was accomplished using middle tension M(T) specimens. The following conclusions can be drawn on the basis of the study;

(1) The extruded material was composed of recrystallized grains. In the longitudinal direction, clusters of constituent particles were found aligned along the direction of extrusion.

(2) Monotonic tensile properties of the material in two directions showed that the yield and tensile strengths were almost the same. However, higher values of elongation and reduction in area were observed in the longitudinal direction.

(3) The fatigue life analysis of the samples in two orientations indicated a shorter fatigue life in CR direction.

(4) The da/dN versus ΔK plot on log-log scale showed a typical sigmoidal shape. The fatigue crack growth rate in the CR orientation was higher as compared to LR orientation.

(5) For the CR orientation, the Paris constants C (m/cycle) and m were found to be 4 x 10^{-11} and 3.4, respectively. The same constants for the LR orientation were found to be 2 x 10^{-10} and 2.6, respectively.

(6) Post fracture analysis revealed that the fracture appearance changed with the sample orientation. The general mechanism of crack growth was the formation of striations.

(7) The present study revealed that the texture of the constituent particles created during extrusion process has a pronounced effect on the crack growth rate in two orientations.

Acknowledgement

The authors are highly indebted to the College of Electrical & Mechanical Engineering, National University of Sciences and Technology, Rawalpindi, Pakistan, for the support during this research work. Thanks are due to Mr. Arif Hussain for his help in fatigue testing.

References

[1] A. Merati, A study of nucleation and fatigue behavior of an aerospace aluminum alloy 2024-T3, Int. J. Fatigue 27 (2005) 33-44.

[2] L. Molent, R. Jones, S. Barter and S. Pitt, Recent developments in fatigue crack growth assessment, Int. J. Fatigue 28 (2006) 1759-1768.

[3] R. I. Stephens, A. Fatemi, R. R. Stephens and H. O. Fuchs, Metal Fatigue in Engineering, second ed., John Wiley & Sons, Inc., New York, (2001).

[4] I. J. Polmear, Light alloys: metallurgy of the light metals, second ed., London: Edward Arnold, (1989).

[5] A. Heinz, A. Haszler, C. Keidel, S. Moldenhauer, R. Benedictus and W. S. Miller, Recent development in aluminum alloys for aerospace applications, Mater. Sci. Eng. A280 (2000) 102-107.

[6] L. P. Borrego, J. M. Ferreira, J. M. Pinho da Cruz and J. M. Costa, Evaluation of overload effects on fatigue crack growth and closure, Eng. Fracture Mech. 70 (2003) 1379-1397.

[7] T. Oppenheim, S. Tewfic, T. Scheck, V. Klee, S. Lomeli, W. Dahir, P. Youngren, N. Aizpuru, R. Clark Jr., E. W. Lee, J. Ogren and O. S. Es-Said, On the correlation of mechanical and physical properties of 6061-T6 and 7249-T76 aluminum alloys, Eng. Fail. Anal. 14 (2007) 218-225.

[8] E. A. DeBartolo and B. M. Hillberry, A model of initial flaw sizes in aluminum alloys, Int. J. Fatigue 23 (2001) S79-S86.

[9] D. Sigler, M. C. Montpetit and W. L. Haworth, Metallography of fatigue crack initiation in and overaged high-strength aluminum alloy, Metal. Trans. 14A (1983) 931-938.

[10] A. Zabett and A. Plumtree, Microstructural effects on the small fatigue crack behavior of an aluminum alloy plate, Fatigue Fract. Eng. Mater. Struct. 18 (1995) 801-809.

[11] M. A. Fonte, S. E. Stanzl-Tschegg, B. Holper, E. K. Tschegg and A. K. Vasudevan, The microstructure and environment influence on fatigue crack growth in 7049 aluminum alloy at different load ratios, Int. J. Fatigue 23 (2001) S311-S317.

[12] K. S. Al-Rubaie, E. K. L., Barroso and L. B. Godefroid, Fatigue crack growth analysis of pre-strained 7475-T7351 aluminum alloy, Int. J. Fatigue 28 (2006) 934-942.

[13] S. E. Stanzl-Tschegg and H. Mayer, The microstructure and environment influence on fatigue crack growth in 7049 aluminum alloy at different load ratios, Int. J. Fatigue 23 (2001) S231-S237.

[14] J. Schijve, M. Skorupa, A. Skorupa, T. Machniewicz and P. Gruszczynski, Application of the strip-yield model from the NASGRO software to predict fatigue crack growth in aluminum alloys under constant and variable amplitude loading, Int. J. Fatigue 26 (2004) 1-15.

[15] P. S. Pao, H. N. Jones, S. F. Cheng and C. R. Feng, Fatigue crack propagation in ultrafine grained Al–Mg alloy, Int. J. Fatigue 27 (2005) 1164-1169.

[16] T. Zhaia, X. P. Jiang, J. X. Li, M. D. Garratt and G. H. Bray, The grain boundary geometry for optimum resistance to growth of short fatigue cracks in high strength Al-alloys, Int. J. Fatigue 27 (2005) 1202-1209.

[17] X. F. Liu, S. J. Huang and H. C. Gu, Crack growth behavior of high strength aluminum alloy in 3.5% NaCl solution with corrosion inhibiting pigments, Technical note, Int. J. Fatigue 24 (2002) 803-809.

[18] N. Kamp, N. Gao, M. J. Starink and I. Sinclair, Influence of grain structure and slip planarity on fa-

tigue crack growth in low alloying artificially aged 2xxx aluminium alloys, Int. J. Fatigue 29 (5) (2007) 869-878.

[19] O. Hatamleh, J. Lyons and R. Forman, Laser and shot peening effects on fatigue crack growth in friction stir welded 7075-T7351 aluminum alloy joints, Int. J. Fatigue 29 (2007) 421-434.

[20] M. Skorupa, T. Machniewicz and J. Schijve, A. Skorupa, Application of the strip-yield model from the NASGRO software to predict fatigue crack growth in aluminum alloys under constant and variable amplitude loading, Eng. Fract. Mech. 74 (2007) 291-313.

[21] S. Suresh, A. K. Vasudevan and P. E. Bretz, Mechanisms of slow fatigue crack-growth in high-strength aluminum alloys – role of microstructure and environment, Metal. Trans. A15 (1984) 369-379.

[22] J. X. Li, T. Zhai, M. D. Garratt and G. H. Bray, Four-point-bend fatigue of AA 2026 aluminum alloys, Metall. Mat. Trans. 36A (2005) 2529-2539.

[23] ASTM standard E 647, Annual book of ASTM Standards. Philadelphia (PA): American Society for Testing and Materials (1996).

[24] M. Staat and D. K. Vu, Limit loads of circumferentially flawed pipes and cylindrical vessels under internal pressure, Int. J. Pressure Vessels Piping 83 (2006) 188-196.

Dr. M. A. Malik is a Professor in Department of Mechanical Engineering, College of Electrical and Mechanical Engineering, National University of Sciences and Technology, Rawalpindi, Pakistan. He graduated from Georgia Tech, USA with MS and PhD degrees in nuclear engineering. He has considerable working experience in nuclear research industry. He specializes in impurity transport and modeling and simulation techniques. His current research interests include structural analysis, reliability of materials and modeling and simulation of dynamic engineering systems. He has over 85 publications to his credit.